J Appl Electrochem (2012) 42:763–777
DOI 10.1007/s10800-012-0443-z

ORIGINAL PAPER

Fundamental studies of sonoelectrochemical nanomaterials preparation

P. Sakkas · O. Schneider · S. Martens · P. Thanou · G. Sourkouni · Chr. Argirusis

Received: 6 March 2012 / Accepted: 29 June 2012 / Published online: 25 July 2012

Abstract The coupling of electrochemical processes and ultrasound has found a larger number of applications during the past years. Especially in the field of materials science and energy technology its potential for the production of nanomaterials, improved metals, alloys and composites is noteworthy. In this paper the focus is on fundamental studies applying the electrochemical quartz crystal microbalance technique in order to improve understanding of these sonoelectrochemical processes. Three examples from the work of the authors in the area are presented: A study of the modification of the electrodeposition of Cu from chloride-based electrolytes by ultrasound, the deposition of metal/ceria composites from electrolytes low in ceria content, and the deposition of metal nanoparticles for decoration of solid oxide fuel cell anode powders. In the first two examples the electrochemical quartz crystal microbalance technique is applied in situ, whereas in the latter example it was used to study the electrochemistry of the systems involved.

Keywords Sonoelectrochemistry · Ultrasound · Nanoparticles · Fuel cells · Electrochemical quartz crystal microbalance · Metal ceramic composites · Electrodeposition

In memoriam of our esteemed colleague and sonoelectrochemist Prof. José González-Garcia.

P. Sakkas · O. Schneider · S. Martens · P. Thanou · Chr. Argirusis
Institute of Metallurgy, Clausthal University of Technology, Robert-Koch-Str. 42, 38678 Clausthal-Zellerfeld, Germany

P. Sakkas · G. Sourkouni · Chr. Argirusis
Energy Research Centre Lower Saxony, Clausthal University of Technology, Am Stollen 19, 38640 Goslar, Germany

P. Sakkas · P. Thanou · Chr. Argirusis
Laboratory of Inorganic Materials Technology, Department of Synthesis and Development of Industrial Processes, National Technical University of Athens, 9, Heroon Polytechniou St, 15780 Zografou, Greece

O. Schneider (✉)
Department of Physics, Chair for Energy Conversion and Storage, Technische Universität München, E19, James-Franck-Str. 1, 85748 Garching, Germany
e-mail: oliver_m.schneider@tum.de

G. Sourkouni
Institute of Electrical Power Engineering, Clausthal University of Technology, Leibnizstraße 28, 38678 Clausthal-Zellerfeld, Germany

1 Introduction

The application of ultrasound in chemistry both for cleaning purposes and for acceleration of existing and introduction of new chemical reactions and processes is well established. Nevertheless, in recent years an upsurge in the field of sonochemistry and exploration of new fields of application has been observed. The concept was applied to electrochemical reactions as well, and several reviews on the emerging field of sonoelectrochemistry have been published [1–4]. Ultrasound has been applied in the fields of electroplating, electroorganic synthesis, electropolymerisation, electroanalytical chemistry and for the electrochemical production of nanoparticles [1–4].

One of the major effects of ultrasound propagation in a liquid medium is acoustic cavitation. There are a number of good reviews covering this phenomenon, but the processes are still not entirely understood [5–8]. During the negative pressure phase small bubbles can be formed either because the cohesive forces of the solvent are overcome by the negative acoustic pressure or due to the presence of

dissolved gas clusters in solution. One distinguishes between stable cavitation and transient cavitation [3, 6, 9]. High speed photography studies on single bubbles in an acoustic trap have shown that those bubbles "slowly" grow during the rarefaction cycle, and rapidly collapse in the compression cycle. During the collapse the temperature within the bubble rises to values of up to 15,000 K. In transient cavitation, the rest radius of the bubble grows from one period of ultrasound to the next one by rectified diffusion [6, 8]. During the growth phase of the bubble more solvent vapor enters the cavity than is condensed during the compression cycle. The bubbles grow to sizes of 5–20 μm [10, 11]. At some point, the bubble experiences a violent collapse connected with a local increase of temperature to values of a few thousand K, very high pressures, high heating and cooling rates and, in the immediate surroundings of the bubble, strong shock waves (hot spot theory) [6, 12]. Due to the instability of the collapsing bubble surface liquid jets directed to the bubble interior form [13]. In the vicinity of a surface the symmetry of the collapse is disturbed and the jet is directed towards the surface. This liquid jet as well as the shock waves can erode the surface [3, 12], even though there has been a report doubting the existence of these directed jets at ultrasound frequencies [14]. Another important effect caused by ultrasound is acoustic streaming [9, 15–17]. It is the analogue of the so-called quartz wind, and caused by momentum transfer of the propagating ultrasonic wave to the medium, converting acoustic energy of the sound wave into kinetic energy of the medium. Therefore a strong, non-laminar convection of the liquid medium in the direction of the propagating wave is taking place in the area, where ultrasound enters the medium.

Sonoelectrochemical experiments can be conducted in many ways differing by how ultrasound is introduced in the system, the geometry of the setup including the arrangement of electrode and ultrasonic transducer, and intensity and frequency of the ultrasound. Using ultrasonic horn probes the working electrode can be placed at a fixed distance in line with the ultrasonic horn probe such that the electrode surface and the surface of the probe tip are parallel, and that the ultrasonic wave is moving towards the electrode. This is the so-called face-on geometry [18]. The acoustic streaming is then directed towards the electrode. Alternatively, the ultrasonic horn tip can directly serve as the electrode [19], and then is called a sonotrode. The latter technique enables a facile way for the production of nanoparticles by a combination of current and ultrasound pulsing [19–24]: a short current pulse under silent conditions leads to the deposition of small nanocrystals of a metal on the horn tip surface. These are then removed by an ultrasound pulse from the sonotrode and therefore can no longer grow. Addition of surfactants might then stabilize the nanoparticles in suspension. Repetition of the procedure allows production of larger numbers of nanoparticles. This technique has been applied to a number of different metals. Recent reviews are available in literature [25–27].

Electrochemistry is of great significance in the field of energy conversion, and might contribute to a more sustainable production of electric and mechanical energy. Electrochemical processes are at the heart of fuel cells and batteries that are important for the large scale market introduction of electric vehicles [28], but also of interest for stationary power applications. Electrochemical processes, however, can also be used to synthesize and modify different components of these devices. This concerns the electrochemical synthesis of nanoparticles for catalysis in low temperature fuel cells or for modification of cermets in high temperature fuel cells, the direct electrodeposition of metal-ceramic composites (even though for high temperature fuel cells these are currently prepared in different ways), and the electrochemical preparation of new battery materials. The combination with ultrasound expands the options considerably. There are also a number of environmental applications for sonoelectrochemistry, like the treatment of industrial waste waters [29–31] and the enhancement of electroanalytical techniques for the detection of pollutants [32] and for process control, and improved metal recycling [33]. Several electrosynthesis reactions can be done in a more environmentally friendly way. An example is the electropolymerisation of water-insoluble monomers from aqueous electrolytes [34].

Ultrasound is also beneficial for the electrochemical deposition of composites [35–37]. In the simplest case metal-ceramic composites can be prepared by the incorporation of oxides dispersed in the electrolyte during electroplating of metals (electrocodeposition). Here ultrasound has been applied in literature for the desagglomeration of particles both by pretreatment of the deposition suspensions before and during the electrodeposition process [36, 38, 39]. In addition the directional movement of the oxides due to acoustic streaming might enhance transport of the oxides to the electrode.

A very valuable method in electrochemistry is the electrochemical quartz crystal microbalance technique that permits to derive mass changes of the electrode during electrochemical reaction with high sensitivity. Recently we have shown that this technique can also be applied in the presence of ultrasound, as long as the cavitation at the surface is not too strong [35, 37, 40]. In this paper we give three examples for this technique: First fundamental studies of the sonoelectrochemical deposition of Cu from chloride based electrodes are shown to demonstrate the technique. Thereafter the deposition of metal/ceria composites from electrolytes low in ceria content is discussed. Finally it is shown that the technique can be used to learn more about the electrochemistry of electrolyte mixtures

typically used for the sonoelectrochemical preparation of colloidal metal solutions. The application of such colloidal solutions for decoration of solid oxide fuel cell anode powders is demonstrated.

2 Experimental

The experimental setup used for all experiments has been discussed in detail elsewhere [40]. A 10 MHz quartz resonator with Au electrodes on both sides was mounted in the bottom of an electrochemical cell, so that one of the Au electrodes was exposed to the electrolyte and served as the working electrode (WE). An ultrasonic horn probe (full wavelength probe, 20 kHz, 13 mm diameter) with a planar exchangeable tip (area 1.2 cm^2) was placed at a distance between 8 and 22 mm above the WE in the face-on geometry. In parallel to the electrochemical experiments the horn probe was operated at different amplitudes (0–100 % of maximum amplitude) by an ultrasonic processor (Sonics VCX 750 or Bandelin SONOPULS HD 3200). A saturated Ag/AgCl electrode ($E_0 = 0.197$ V vs. NHE [41]) served as reference electrode (RE), and all potentials quoted in this paper are referred to it. A platinum-plated titanium wire electrode served as counter electrode. All Cu deposition/dissolution experiments in this study were performed in electrolyte solutions with an initial composition of 0.01 M $CuCl_2$, 0.5 M NaCl, and pH ~1. The pH was adjusted by addition of hydrochloric acid. Background currents were checked by conducting sonoelectrochemical measurements in an electrolyte of 0.5 M NaCl with pH ~1. The entire setup was placed in an Ar-filled glove bag. The cell was continuously purged with Ar during and in between experiments. Ar purging was stopped for the duration of the experiment during measurements without ultrasound. An analogous setup was used for the experiments on Co and Co/ceria composite deposition. Co deposition was performed from a concentrated electrolyte (1 mol l^{-1} $CoSO_4 \cdot 7H_2O$, 0.2 mol l^{-1} $CoCl_2 \cdot 6H_2O$, 0.28 mol l^{-1} H_3BO_3, 0.4 g l^{-1} SDS (sodium dodecylsulfate, pH ~ 4.5) and a less concentrated one (0.1 M $CoSO_4$ + 0.1 M Na_2SO_4 with pH adjusted to 4, based on [42]), both at 25 °C. For codeposition of ceria 0.5–5 g l^{-1} gadolinia doped ceria (Fuel Cell Materials, 5–10 nm crystallite size, softly agglomerated, particle size <149 μm) were added to the electrolyte and treated for 20 min with ultrasound in order to break up the agglomerates. Electrodeposition was as well carried out in the presence of ultrasound. The ultrasonic intensity (I_a) was determined using the calorimetric calibration procedure [43, 44]. Prior to depositions cyclic voltammetry at a scanrate of 5 mV s^{-1} and at different ultrasonic amplitudes was performed in order to characterize the electrochemical behavior of the systems. The deposit thickness was determined by profilometry (Tencor Alpha-Step 500 Surface Profiler). The ceria content in the deposits was determined by electron probe microanalysis (EPMA) and EDX, and the morphology characterized by scanning electron microscopy (SEM).

The electrochemical measurements (cyclic voltammetry and galvanostatic transients) were controlled by a Solartron SI1287 electrochemical interface. Electrical currents measured were converted to current densities by normalizing it to the area of the WE electrode exposed to the electrolyte. In parallel to the sonoelectrochemical measurements the electrical admittance spectra of the quartz resonator were measured in the vicinity of its resonance frequency using an Agilent E5100A network analyzer, which had been calibrated before the measurements using a "thru"-calibration (short-circuit) in the entire frequency range applied later on during electrochemistry. The resonance frequency of the quartz f_R and its damping w were determined after the experiments from the spectra by fitting the real part of the admittance to a Lorentz function. From the frequency shift Δf_R the change in mass density and therefore the amount of material deposited or dissolved was calculated according to the Sauerbrey Eq. (1) (f_0: resonance frequency of bare quartz, $Z_Q = 8.849 \times 10^5$ g cm^{-2} s^{-1} is the mechanical impedance of the quartz) [45]. Potentiostatically deposited layers were characterized by scanning electron microscopy.

$$\Delta f_R = -\frac{2f_0^2}{Z_Q}\frac{\Delta m}{A} \tag{1}$$

Typical solution compositions for the preparation of Ag, Au and Cu nanoparticles are given in Table 1. Polyvinylpyrrolidone (PVP) was added as a stabilizer in order to prevent agglomeration of the as-formed nanoparticles, does however also affect the mechanism of electrodeposition [46, 47]. These effects were studied by fundamental EQCM studies in the same setup. A different setup however was used for the actual sonoelectrochemical preparation of metal nanoparticles. In this case, the circular face of the cylindrical ultrasound transmitting horn itself served as the working electrode. The cylindrical periphery of the WE was electrically insulated from the electrolyte solution. A glass cell from Pine instruments was used for the experiment. Temperature was kept constant at 25 °C. All

Table 1 Representative electrolyte compositions for nanoparticle preparation

Metal	Composition	Reference
Ag	$AgNO_3$ (5 mM)/PVP (20 g l^{-1})/$NaNO_3$ (0.1 M)	[46]
Cu	$CuSO_4 \cdot 5H_2O$ (0.1 M)/PVP (2 wt%)/H_2SO_4 (pH ~ 0)	[47]
Au	$HAuCl_4 \cdot 3H_2O$ (2.8×10^{-4} M)/PVP (20 g l^{-1})/HCl (pH ~ 1)	[48]

experiments were carried out under Ar atmosphere. Galvanostatic (or potentiostatic) conditions for metals reduction at the WE were controlled by an IVIUM CompactStat potentio-/galvanostat (boosted by the PlusModule) and ultrasonic pulses were generated by a Bandelin SONOPULS HD 3200 utilizing a 200W ultrasound generator and a sonication extension horn of 13 mm diameter. The amplitude has been fixed to 10 % in all experiments presented in the present study. Both the Ivium potentiostat and the Bandelin control unit were controlled by a computer. Metal nanoparticles preparation was based on a synchronised action of a periodic galvanostatic deposition (transient chrono-potentiometry, TCP) or potentiostatic deposition (transient chrono-amperometry, TCA) leading to the formation of nanoparticles on the horn face coupled with a subsequent ultrasonic burst for removal of the reduced metal from the ultrasound horn. The general principle is shown in Fig. 1.

The as-prepared nanoparticle-containing solutions were characterized with respect to particle size distribution by dynamic light scattering (DLS) technique using a Zetasizer Nano (Malvern). Small amounts of the solutions were transferred to cuvettes for the measurements. The instrument delivers information on intensity weighted distributions. Information about the suspension medium (e.g., water) as well as the particle (e.g., Cu) refractive index (RI) need to be provided for conversion from intensity to number weighted distribution by use of the Rayleigh and Rayleigh–Gans–Debye (RGD) theory. For particles small compared to the laser wavelength this can be neglected. The RGD approach can be used for $d < \lambda/2$ and Rayleigh

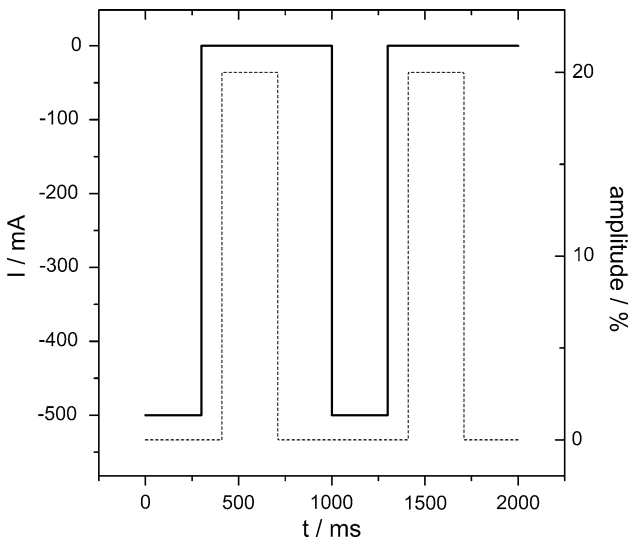

Fig. 1 Synchronization principle of ultrasonically aided galvanostatic nanoparticle generation. Current signal (*solid line*). Ultrasound signal (*dashed line*). The time span for which current was turned on will be denoted as t_{el} and the one of ultrasound t_{US}

for even smaller particle sizes. As the wavelength of the used laser is 633 nm the RGD approach can be used for particles with maximum diameter of ca. 300 nm [49]. If the particles are in the range of $\lambda/10$ then the Rayleigh approach is valid and one can convert intensity weighted to number weighted distribution with even less inaccuracy for particle diameter even up to 100 nm.

Anode powders (cermet of NiO and gadolinium doped ceria, GDC) for decoration with nanoparticles were prepared using the combustion method by Dpto. de Vidrios, Instituto de Cerámica y Vidrio, CSIC, Madrid, Spain.

3 Results

3.1 Electrodeposition of Cu from chloride-based electrolytes in the presence of ultrasound

Cyclovoltammetric experiments were performed at electrode-horn separations of 8, 10, 15, and 22 mm using the electrochemical quartz crystal microbalance technique (EQCM). However, the applicability of the acoustic-wave based and very sensitive EQCM technique in the presence of power ultrasound is not self-evident. Nevertheless, in recent publications we showed that the method indeed can be applied at least under the conditions of acoustic streaming [35, 37, 40], when cavitation at the electrode surface is absent. An excess of chloride (0.5 mol l^{-1}) was used in order to prevent the formation of solid CuCl on the electrode. Typical cyclic voltammograms and the frequency response of the quartz resonator under silent conditions and at ultrasonic intensities of 14 and 76 W cm^{-2} (15 mm distance) are shown in Fig. 2. Under silent conditions (Fig. 2a), both peak couples known from literature have been reproduced. Frequency changes due to Cu deposition and dissolution were only observed for the peak pair at lower potentials. In agreement with literature data [50–52] the peak pair at higher potentials was assigned to the Cu^{2+}/Cu^{+}-redox couple, and the one at lower potentials to Cu deposition and dissolution. The total charge per cycle was negative because only part of Cu(II) reduced to Cu(I) is re-oxidized thereafter. Already under a rather low ultrasonic intensity I_a the shape of the voltammogram severely changed (Fig. 2b), and both cathodic peaks and the anodic peak of Cu(I)/Cu(II) oxidation disappeared. In the potential range above 0.1 V anodic and cathodic current traces now were found to be nearly identical. The currents became slightly positive at elevated potentials, but there was no more anodic peak in that region. At potentials below 0.3 V the current became negative and its magnitude increased almost linearly with decreasing potential, the slope di/dE increasing with I_a. At 8 W cm^{-2} and $d = 22$ mm it finally leveled off. There was little if any

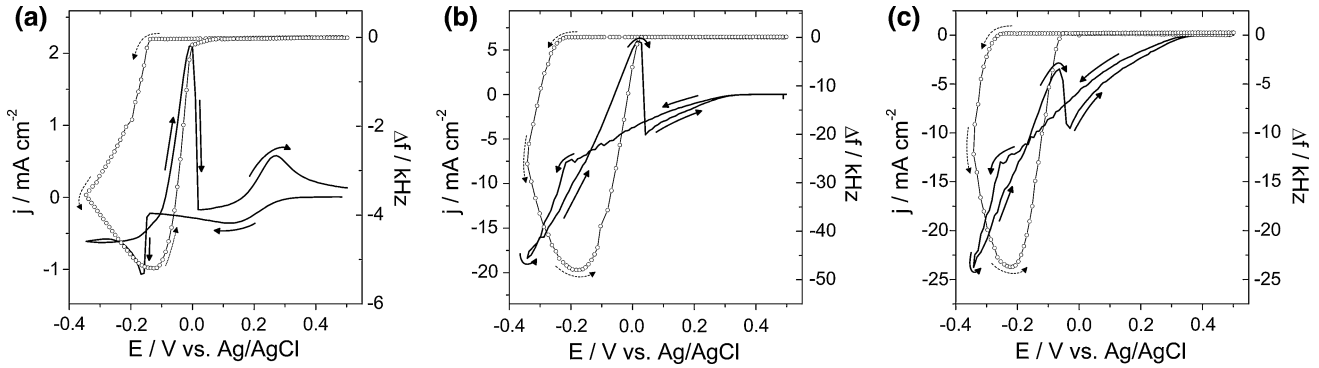

Fig. 2 Electrochemical deposition and dissolution of Cu from an electrolyte of 0.01 M $CuCl_2$ + 0.5 M NaCl, pH ~ 1 **a** under silent conditions and at $d = 15$ mm under an ultrasonic intensity of **b** 14 W cm^{-2} and **c** 76 W cm^{-2}. *Lines* current density at the Au working electrode (WE). *Circles* frequency changes of quartz resonator. *Arrows* indicate direction of potential sweeps, sweep rate 0.005 V s^{-1}

influence of I_a on the potential where the corresponding reduction process set in. At $I_a > 9$ W cm^{-2} the cathodic currents continued to increase linearly until Cu deposition started (Fig. 2b, c). With increasing intensity the entire voltammogram was found to shift into the negative current region (Fig. 2c).

The potential where Cu deposition began was determined from Δf_R and clearly shifted in the presence of ultrasound and with increasing I_a to more negative values. Ultrasound of low intensity increased maximum cathodic currents and the amount of Cu deposited on the quartz by a factor of ten or more. A further increase in ultrasonic intensity still caused an increase in the maximum cathodic current densities, but the anodic peak currents decreased in magnitude, finally becoming negative, and less Cu was deposited. After correction for the background currents the anodic peak currents were positive, but still decreased with I_a, because the smaller amount of Cu deposited led to lower maximum dissolution currents. From the total mass Δm deposited and the total cathodic charge flux ΔQ an averaged (apparent) current efficiency ε for the deposition (assuming $z = 2$), and from the anodic peak charge (after background correction, assuming $z = 1$) for the dissolution was calculated from Eq. (2) (Fig. 3). For the deposition process ε was found to be far below 1, and to decrease further with increasing I_a. For the dissolution the ε values were >1.

$$\varepsilon = -\frac{\Delta m}{\Delta Q}\frac{zF}{M} \qquad (2)$$

Potential-resolved current efficiencies ε were calculated assuming $z = 1$ (Fig. 4). The shapes of the curves for Cu dissolution were similar with and without ultrasound, starting out at very large numbers and then decreasing with continuing dissolution. The ε-curves for Cu deposition under silent conditions were similar to those reported in sulfate-based electrolytes [40]: ε started at large values, and

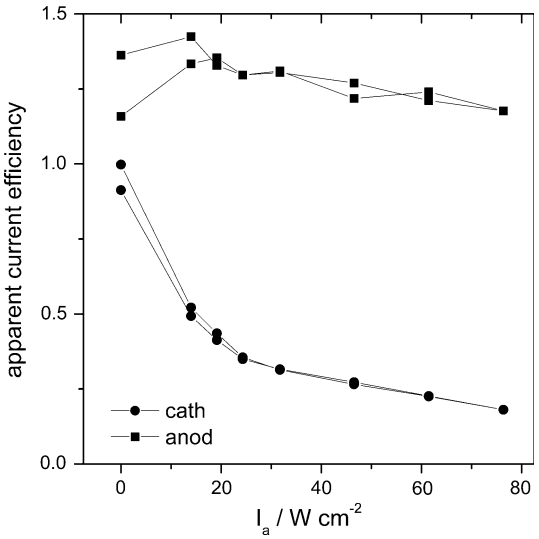

Fig. 3 Averaged cathodic (*circles*) and anodic (*squares*) apparent current efficiencies during Electrochemical deposition and dissolution of Cu from an electrolyte of 0.01 M $CuCl_2$ + 0.5 M NaCl, pH ~ 1 at $d = 15$ mm and sweep rate = 0.005 V s^{-1}

decreased while lowering the potential. After potential reversal ε finally became negative. With ultrasound, though, ε started at zero, and then increased with decreasing potentials. The behavior after potential reversal was similar like under silent conditions. At low potentials ε was nearly constant around 0.5, but decreased at higher I_a. At higher I_a, ε for the anodic process was negative, because the current remained negative even during Cu dissolution.

3.2 Sonoelectrochemical deposition of metal/ceria composites

The electrodeposition of metals reinforced with micron-sized and in part also nano-sized ceramic particles of Al_2O_3, SiO_2, SiC, TiO_2, CeO_2, ZrO_2, borides and others has been state of the art for many decades [53]. Such

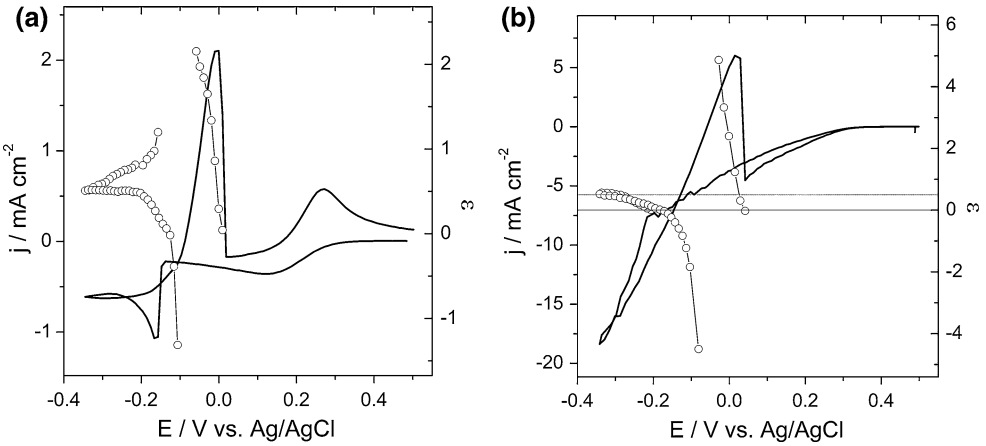

Fig. 4 Electrochemical deposition and dissolution of Cu from an electrolyte of 0.01 M $CuCl_2$ + 0.5 M NaCl, pH ~ 1 at $d = 15$ mm and 0.005 V s^{-1} currents (*lines*) and instantaneous apparent current efficiencies (*circles*) **a** under silent conditions **b** at $I_a = 14$ W cm^{-2}

metal/ceramic composites often show superior corrosion resistance [54]. Other major fields of application have been the improvement and tailoring of the mechanical properties, like hardness (dispersion hardening), yield strength, resistance to plastic deformation and wear resistance, and lubrication of metals by codepositing graphite or PTFE, or liquid lubricant filled microcapsules [54].

The deposition of ceria containing metals has been studied to a lesser extent than the incorporation of Al_2O_3 and others. Ni/ceria and Co/ceria composites are interesting in the context of high temperature fuel cells [55]. In SOFCs Ni/ceria is one option for the anode. Those cermets are characterized by a large concentration of ceria and are typically made by non-electrochemical methods. Ni or Co/CeO_2 are however also candidates to protect the cathode in molten carbonate fuel cells, and in this respective electrochemical deposition methods are of interest. Carac et al. [56] incorporated μ-sized ceria particles from Watts-type electrolytes in Ni and Co without using ultrasound and registered an increase in microhardness. Lee et al. [36] applied ultrasound during the preparation of Cu/Al_2O_3 and Cu/CeO_2 composites, but not in the face on geometry. They found that ultrasound was less efficient in breaking up agglomerates in the case of ceria. Lampke et al. [57] performed the electrodeposition of Ni/TiO_2 and Ni/Al_2O_3 deposits in an ultrasonic bath. Qu et al. [58] treated the electrolyte with ultrasound before electrodeposition of Ni/ceria composites.

The study of the electrochemical deposition of both Co/ceria as well as Ni/ceria from electrolytes with low CeO_2 loading under the influence of ultrasound in combination with EQCM has been discussed in two previous publications [35, 37]. Therefore here only some specific points shall be summarized, focusing entirely on the Co system. First the influence of ultrasound on cyclic voltammetry in absence and presence of ceria will be discussed. Thereafter the different morphologies obtained under the influence of ultrasound for pure Co layers from different electrolytes will be compared. Finally the codeposition of ceria is shortly summarized.

For the deposition of Co and Co/ceria composites large differences are observed based upon the electrolyte. Cyclic voltammograms for the Watts type Co electrolyte and the low concentration electrolyte are shown in Fig. 5. Both show the influence of nucleation and growth processes: the deposition currents are larger in the backward sweep than in the forward sweep, and a so-called trace crossing can be observed. In a Watts-type Co electrolyte cyclic voltammetry in the absence of ultrasound showed average efficiencies of 90 % for deposition and 93.5 % for the dissolution, as determined by the total cathodic and anodic charges and the corresponding mass changes. Also the charges of dissolution (0.211 C cm^{-2}) and deposition (0.216 C cm^{-2}) are very close to each other, indicating that the deposit is fully dissolved during the backward scan of the voltammogram. This observation is confirmed by the frequency changes of the quartz resonator that return to the original values after the end of the dissolution process. In the second, more dilute electrolyte without borate buffer the situation changes significantly: There is already an electrochemical process taking place at electrode potentials positive of the onset of bulk Co deposition, as clearly indicated by the decrease in frequency and cathodic current densities measured in this region. The actual deposition currents are somewhat smaller than in the concentrated electrolyte, which is expected. However, the average current efficiency for deposition is 108 %. The dissolution charge (0.102 C cm^{-2}) is much smaller than the deposition charge (0.193 C cm^{-2}). The average current efficiency during the dissolution process is 112 %. Only half of the deposit formed during the cathodic part of the voltammogram is removed during the anodic sweep. At very positive potentials an increase in the current and an increase in resonance frequency can be seen, indicating another dissolution process. The apparent efficiency for this process based on Co dissolution is 300 %. It could be shown that

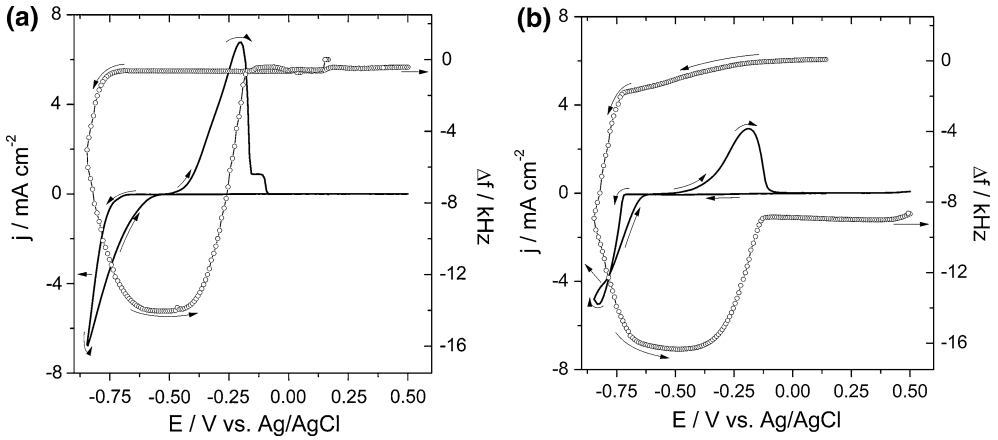

Fig. 5 Cyclic voltammograms under silent conditions (*lines*) and corresponding frequency change (*circles*) of an Au coated quartz resonator at $v = 0.005$ V s^{-1} in **a** 1 mol l^{-1} $CoSO_4{\cdot}7H_2O$, 0.2 mol l^{-1} $CoCl_2{\cdot}6H_2O$, 0.28 mol l^{-1} H_3BO_3, 0.4 g l^{-1} SDS, pH $\sim$ 4.5, **b** 0.1 M $CoSO_4$ + 0.1 M Na_2SO_4, pH $\sim$ 4

extended holding at elevated potentials leads to complete removal of the deposit.

In the presence of ultrasound the maximum deposition currents, the shape of the voltammetric trace in the deposition region and the amount of material deposited become very similar (cf. Fig. 6). In both electrolytes cathodic currents are visible at potentials above the deposition potential, but only in the diluted electrolyte this is connected to a mass change on the electrode. In the dilute electrolyte both the deposition charges and the dissolution charges increase at larger ultrasonic intensities, but this effect is much more pronounced for the dissolution charge. Similarly, the deposited mass shows a slight increase by 30 % for $I_a = 28$ W cm^{-2}, while the dissolved mass increases by 150 %: in the presence of ultrasound basically all material deposited below the deposition potential is removed from the electrode during the anodic sweep. However, the mass removal is split into two processes: the major part of the deposit is removed in parallel to the anodic current peak. The remainder of the mass is removed at slightly more positive potentials. A plot of the mass change dmdt^{-1} versus the potential therefore shows a double peak.

For incorporation of ceria mainly the diluted electrolyte was studied, because the amount incorporated with the concentrated electrolyte was not that large. The addition of ceria to the diluted electrolyte leads again to irreversibility in the frequency response during cyclic voltammetry even in the presence of ultrasound. Figure 7 shows the cathodic currents and the maximum masses deposited in the first cycle as a function of the ultrasonic intensity and the electrolyte composition (Watts-like, diluted pure, dilute + 3 g l^{-1} or 5 g l^{-1} CeO_2). The curves for the ceria-free electrolytes are very similar, showing an increase in current densities in the presence of ultrasound. The amount of deposited mass is somewhat less at small I_a, and then clearly increases with I_a. For the dilute electrolyte with addition of ceria the trend is less clear. There are some changes in current densities, but much smaller than in the absence of ceria. Also no clear tendency for the deposited mass can be seen. Figure 8 shows plots of the mass density in function of the potential for the two first cycles at different ultrasonic intensities for an electrolyte with 5 g l^{-1} CeO_2. The amount of material deposited during the actual deposition process is roughly the same in the first and

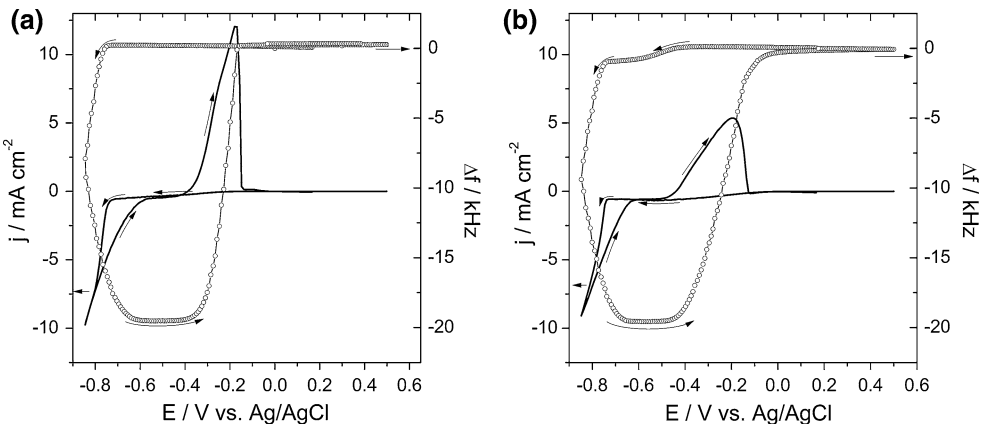

Fig. 6 Cyclic voltammograms (*lines*) and corresponding frequency change (*circles*) of an Au coated quartz resonator at $v = 0.005$ V s^{-1} in the presence of ultrasound at $I_a = 28$ W cm^{-2}, $d = 22$ mm, in **a** 1 mol l^{-1} $CoSO_4{\cdot}7H_2O$, 0.2 mol l^{-1} $CoCl_2{\cdot}6H_2O$, 0.28 mol l^{-1} H_3BO_3, 0.4 g l^{-1} SDS, pH $\sim$ 4.5, **b** 0.1 M $CoSO_4$ + 0.1 M Na_2SO_4, pH $\sim$ 4

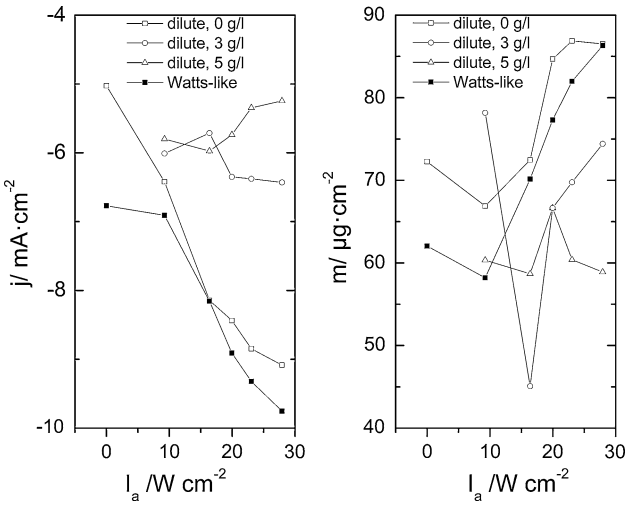

Fig. 7 Maximum cathodic current densities at different ultrasonic intensities in electrolytes of 1 mol l^{-1} $CoSO_4 \cdot 7H_2O$, 0.2 mol l^{-1} $CoCl_2 \cdot 6H_2O$, 0.28 mol l^{-1} H_3BO_3, 0.4 g l^{-1} SDS, pH $\sim$ 4.5 (*filled squares*) and 0.1 M $CoSO_4$ + 0.1 M Na_2SO_4, pH $\sim$ 4 with 0 (*open squares*), 3 (*open circles*) or 5 g l^{-1} (*open triangles*) CeO_2 added

second cycle. However, less than half of the material is removed from the electrode during the anodic dissolution peak. At low ultrasonic intensities only little material is removed at potentials positive of the dissolution peak. At larger ultrasonic intensities, however, a significant portion of the deposit is removed in the potential region where no significant currents are measured.

Depositions for subsequent study of the morphology and CeO_2 incorporation were performed at a constant potential of −0.85 V at an ultrasonic intensity of 28 W cm^{-2}. The amount of material deposited was controlled by setting a predetermined maximum allowable frequency decrease of the resonator. In a Watts-type Co electrolyte the morphology of the deposit obtained was quite compact (Fig. 9) and only a small increase in damping was observed during EQCM (1.1 kHz). On the other hand, the morphology of the ceria-free film deposited from the diluted electrolyte was very different: The entire film consisted of small, rather loose spherical grains. The damping change was correspondingly larger, but still within the range of validity of the Sauerbrey equation (4.7 kHz). The current efficiency determined from the slope of the mass-charge curve from the concentrated electrolyte (90 %) was very similar to the value found for a more dilute electrolyte (93 %). In the presence of 5 g l^{-1} CeO_2 some ceramic material was incorporated in the deposit, but clearly less than with the more dilute electrolyte. The results on the CeO_2 incorporation during potentiostatic deposition from the dilute electrolyte have been shown elsewhere [35]. It was demonstrated that the morphology of the deposits was strongly altered by the presence of ceria, that the films became much rougher and that a rather inhomogeneous distribution across the electrode surface was seen. All these factors caused such a strong increase in the damping that application of Sauerbrey's equation was no longer valid. However, the amounts of ceria embedded were quite large, as determined by EPMA, up to 7.8 % [35].

3.3 Sonoelectrochemical preparation of nanoparticles

The development of solid oxide fuel cells (SOFC) as a viable energy conversion system is still hindered by insufficient durability, especially of the anodic cermet electrode [59]. Utilization of natural gas (NG) or other hydrocarbons (H/C) leads to severe degradation phenomena such as carbon and sulphur poisoning of the cermet matrix [60]. In view of the fact that natural gas and biogas tend to be a key vector in global economy, minimizing

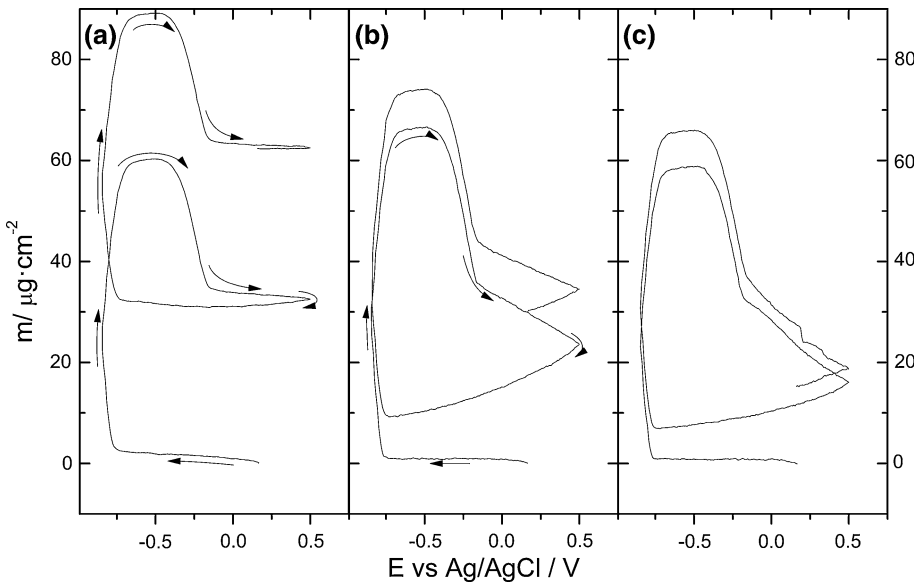

Fig. 8 Mass changes during cyclic voltammetry of an Au coated quartz resonator at $v = 0.005$ V s^{-1} in 0.1 M $CoSO_4$ + 0.1 M Na_2SO_4 + 5 g l^{-1} CeO_2 in the presence of ultrasound at I_a: **a** 9 W cm^{-2} **b** 20 W cm^{-2} **c** 28 W cm^{-2}

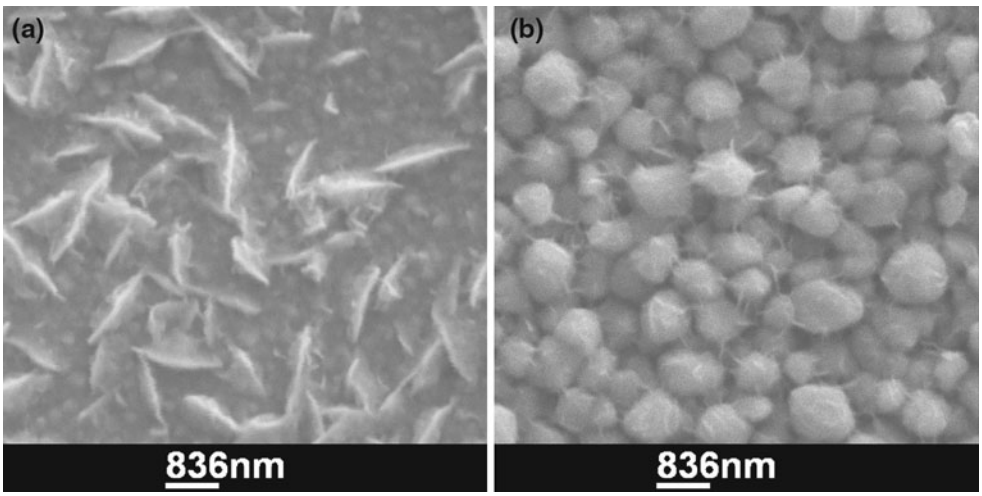

Fig. 9 Morphology of films deposited at $E = -0.85$ V versus Ag/AgCl and $I_a = 28$ W cm^{-2} from **a** 1 mol l^{-1} $CoSO_4 \cdot 7H_2O$, 0.2 mol l^{-1} $CoCl_2 \cdot 6H_2O$, 0.28 mol l^{-1} H_3BO_3, 0.4 g l^{-1} SDS, pH $\sim$ 4.5 **b** 0.1 M $CoSO_4$ + 0.1 M Na_2SO_4, pH $\sim$ 4. Film thickness was controlled by a fixed total frequency shift of -300 kHz

anode degradation in SOFC utilising natural gas or other hydrocarbons is of outmost importance.

Decoration of a Ni-based (state-of-the-art) anode material by metal nanoparticles (NP) is a promising strategy for cermet's fine-tuning. Modification of Ni-based cermets (YSZ/Ni or GDC/Ni) by decorating with Au, Ag or Cu NPs leads to materials able to operate under steam or dry reforming conditions with high C tolerance at intermediate temperatures (IT) [60–63]. Preliminary promising results have been obtained for the cases of Ni/Au and Ni/Ag [63]. Metal particles are usually prepared by chemical reduction of metal salts. Many applications require the production of large quantities of particles with a controlled and uniform size. For making a chemical reduction route versatile enough one has to adjust the reducing agent, the protective substance, the solvent, the temperature or several combinations of these experimental parameters [64]. A general method for nanoparticles preparation of adjustable size with no need of altering experimental conditions such as medium concentration, temperature or ligands is the sonoelectrochemical technique using the sonotrode configuration described above [19, 22]. The achievement of a narrow size distribution is of great importance for this method as well [65]. In the following some results for the deposition of Cu and Au nanoparticles are presented.

3.3.1 *Copper electrochemistry in presence of PVP and nanoparticle deposition*

The presence of PVP alters the electrochemical behaviour even on well conducting, inert electrode substrates like gold (Fig. 10). The deposition process now becomes split up into several processes happening at different potentials. Despite a 10-times larger Cu^{2+} concentration for the voltammogram in Fig. 10b the onset of Cu bulk deposition is shifted to lower potentials. A clear cathodic peak not present in the absence of PVP is observed that is correlated with a frequency decrease and thus a deposition process. Despite a more negative applied potential and a larger Cu concentration less Cu is deposited in the cycle, as seen by the lower overall frequency change.

The typical shape of the potential-time curve during the pulsed galvanostatic deposition of Cu particles on the Ti horn is shown in Fig. 11.

The large applied currents to enforce the particle deposition caused a large overpotential, as seen in the very negative potentials obtained when the current was on. Once the current was turned off, the potential returned into the region of the equilibrium potential for Cu/Cu^{2+} in this electrolyte. The period where the ultrasound is turned on can be identified under certain conditions in the potential time curve, as demonstrated in Fig. 11 by the slight potential increase after turning off the ultrasound. The 300 ms pulse length applied in this experiment, however, was too long. This is demonstrated in Fig. 12 where the particle size distribution for 300 and 50 ms are compared. A lower pulse length reduced the average particle size significantly. A strong dependency of particle sizes on deposition conditions was also obtained for Ag and Au nanoparticles.

3.3.2 *Gold nanoparticles*

Au nanoparticles are of the largest interest for SOFC anode modification. The vast majority of experiments was based on pulsed ($t_{el} = 0.02, 0.05, 0.1, 0.2, 0.3$ and 0.4 s) potentiostatic ($E = -1.5$ and -2 V) conditions along with continuous ultrasonication at low ultrasonic intensities. A few

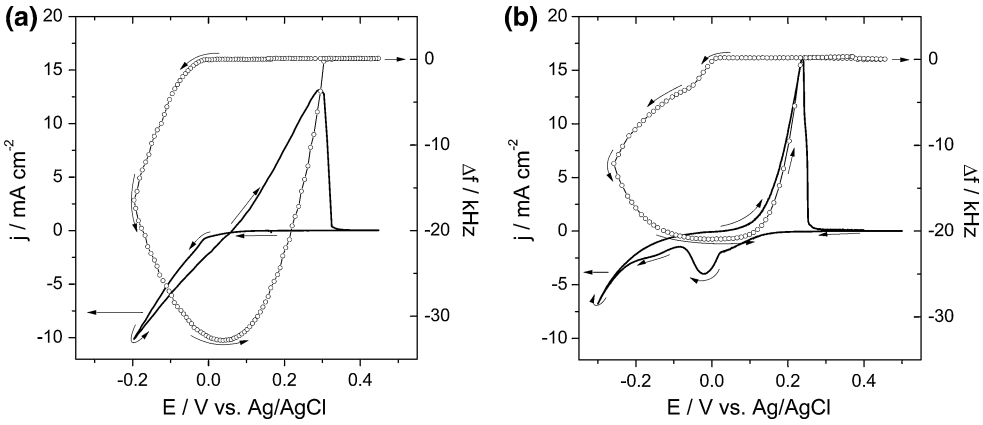

Fig. 10 Cyclic voltammograms and corresponding frequency change of an Au coated quartz resonator at $v = 0.005$ V s^{-1} in the presence of ultrasound at I_a =76 W cm^{-2}, in **a** 0.01 M $CuSO_4$ + 0.1 M Na_2SO_4 of pH $\sim$ 1 at $d = 10$ mm **b** 0.1 M $CuSO_4$ + H_2SO_4 (pH $\sim$ 0) + 2 wt% PVP at $d = 15$ mm

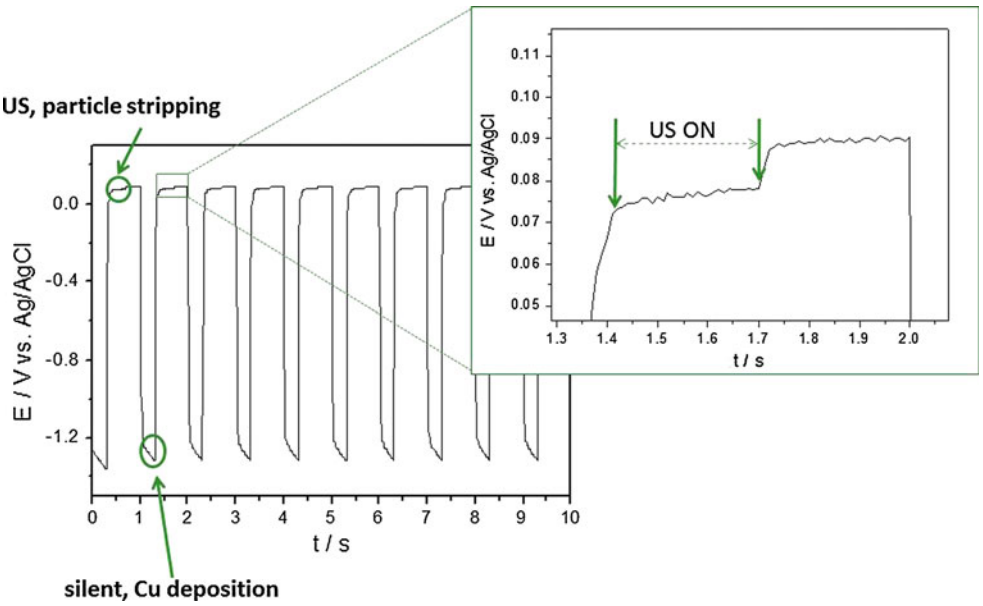

Fig. 11 Pulsed electrodeposition of Cu from the electrolyte listed in Table 1 with $I = -500$ mA, for 300 ms. The time period during which ultrasound (US) was applied (while $I = 0$ mA) is shown in the enlarged graph

experiments were conducted under pulsed ($t_{el} = 0.05$ s) galvanostatic ($I = 0.1$ and 0.06 A) conditions under pulsed ($t_{US} = 0.05$ s) ultrasonication. The novelty introduced in the last experiments is that of continuous ultrasonication and parallel continuous electrodeposition. A characteristic change in the solution color from transparent yellow to transparent magenta showed the formation of nanoparticles, in full analogy to the long-established formation of Au sols by chemical reduction.

In Fig. 13, the first result of 10.2 nm belongs to a replication of the experiment that was found in the recent literature [23]. The remaining results represent our experiments based on continuous ultrasonication at various potentiostatic pulse lengths and one with continuous deposition. The bar chart shows that preparation of Au nanoparticles with diameters in the order of 10 nm has been accomplished.

TEM analysis proved the existence of Au nanoparticles. In Fig. 14 a sample of the experiment with $t_{pulse} = 0.2$ s is depicted. The dark colored islets are Au nanoparticles. Each islet demonstrates different shades of dark grey due to different crystallographic orientation of the crystal planes of each nanoparticle. The brighter grey that surrounds the islets should be of organic matter (i.e., PVP surfactant) as it comes close to the background color (of Carbon layer). This mass seems to interconnect all nanoparticles just as it would be expected based on a growth model suggested in the literature [46, 47].

3.3.3 *Decoration of cermets with Au nanoparticles*

GDC/NiO anode powder was dispersed in a freshly prepared Au NP solution and direct ultrasonication was performed. The ultrasonication was executed at 100 % of the available equipment amplitude using an ultrasonic horn of 6 mm tip diameter. The nanoparticles suspended in the solution are expected to collide on the anode powder surface under the forces evolved due to the cavitation effects that follow of the ultrasonic activity. A change in powder color from pale green (as is) to dark yellow (after co-sonication) is apparent and stable after weeks of the experiments.

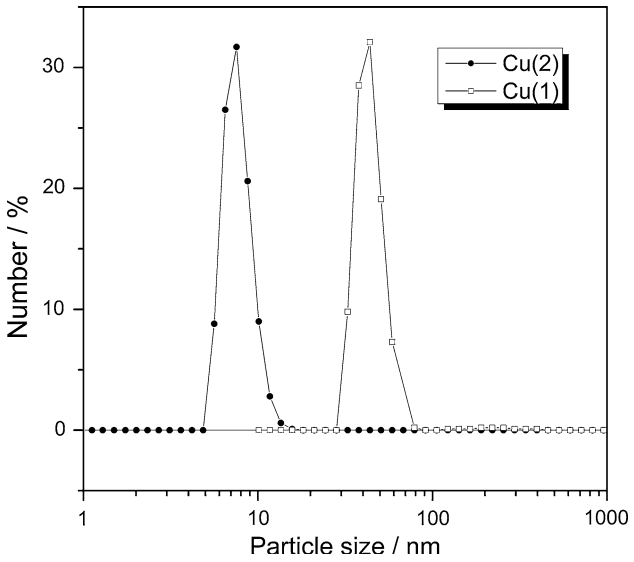

Fig. 12 Particle size distribution of Cu colloidal nanoparticles produced during pulsed sonoelectrochemical deposition from an electrolyte of 0.1 M $CuSO_4 \cdot 5H_2O$, 2 wt% PVP and pH $\sim$ 0 (adjusted with H_2SO_4) solution, lasting 30 min at 15 W cm^{-2} ultrasonic intensity. Cu(1): $I = -500$ mA, $t_{el} = 300$ ms, $t_{US} = 300$ ms, Cu(2): $I = -500$ mA, $t_{el} = 50$ ms, $t_{US} = 100$ ms

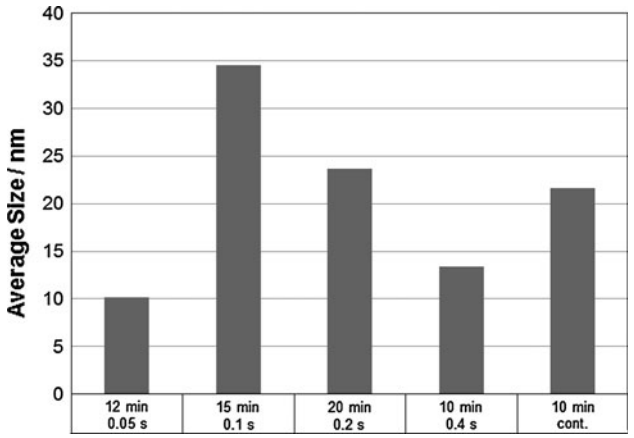

Fig. 13 Particles size distribution of Au nanoparticles in an experiment where the electric pulse duration t_{el} is varied at $E = -1.5$ V versus Ag/AgCl and continuous ultrasound is applied. For the experiment on the *right side* the potential was held constant, i.e., it was not pulsed

Figure 15 shows a SEM figure of the decorated cermet powder. The results from local EDS analysis at several spots are given. Furthermore, several EDS measurements across larger areas yielded $\sim$2 wt% Au, in agreement with the stoichiometry that was intended.

4 Discussion

Electrochemical reaction mechanisms and rates strongly depend on the experimental conditions under which they

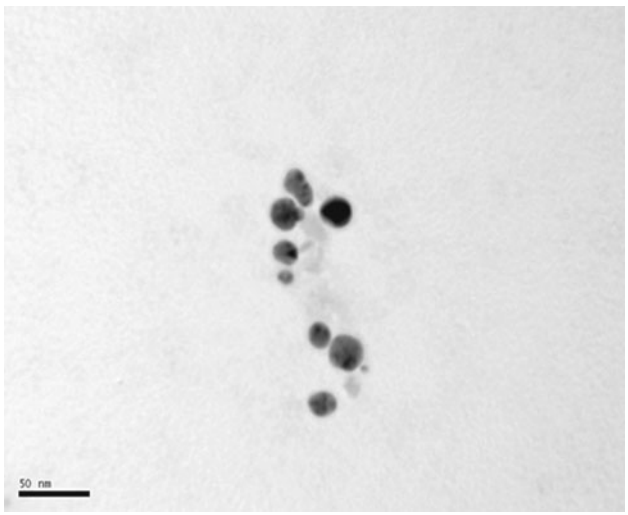

Fig. 14 A TEM image of an Au nanoparticle experiment with $t_{el} = 0.2$ s and $E = -1.5$ V versus Ag/AgCl. The sample was taken after 10 min

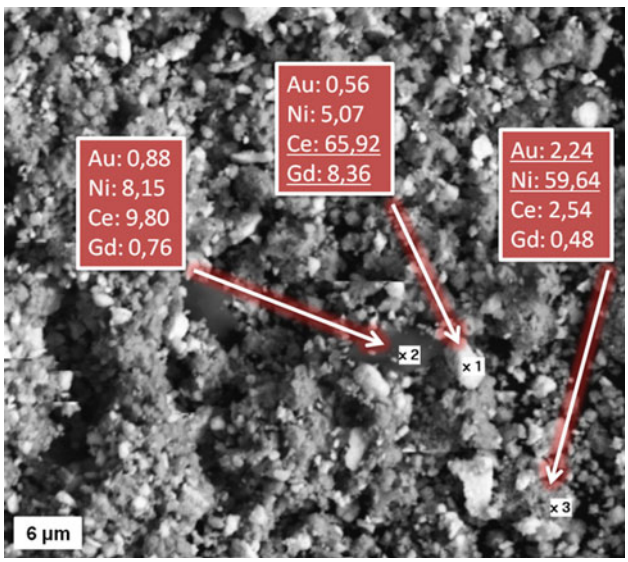

Fig. 15 SEM/EDS analysis of a NiO/GDC anode powder decorated with Au nanoparticles via high power ultrasound at an intended amount of 2 wt%

are carried out. Besides the control parameters electrode potential or applied current, this includes especially the electrolyte composition and the electrode material. While the latter does not play a large role for outer sphere reactions, it is of great importance for reactions involving adsorbed intermediates and for electrodeposition reactions, including the electrochemical formation of nanomaterials. The introduction of ultrasound into such a system expands the range of experimental possibilities, but at the same time the number of independent variables is increased. The controlled formation of nanomaterials by sonoelectrochemical methods can be accomplished by trial and error or

-preferentially—by detailed understanding of the interaction between electrochemistry and ultrasound.

A number of studies on the effects of ultrasound have been performed in literature, and references have been given in the introduction. One method that permits to learn more about electrochemical phase formation and growth is the electrochemical quartz crystal microbalance. It has been demonstrated that this technique can be applied also in the presence of ultrasound. In the current work this method has been applied to the electrodeposition and dissolution of Cu from a chloride based electrolyte and to sonoelectrochemical reactions of importance with respect to the formation of nanomaterials.

In order to understand the observations for the $CuCl_2$ electrolyte, the actual degree of complexation in the electrolyte is important. Based on a potential—log c(Cl^-) diagram for the copper system and the equilibrium constants for the various possible copper species from the paper by Kekesi and Isshiki [50] it was estimated that in the electrolyte used in this work originally 53 % of the Cu(II) should have been present as free Cu^{2+} ions, 41 % as $[CuCl]^+$, and 6 % as $CuCl_2$ (taking the chloride concentration as 0.6 mol l^{-1} and neglecting activity coefficients). The major Cu(I) species formed during repeated cycling should have been $[CuCl_2]^-$ (61 %), followed by $[CuCl_3]^{2-}$ (25 %) and $[CuCl_4]^{3-}$ (6 %). No CuCl precipitation can occur at the high levels of chloride present. Therefore the mass changes under silent conditions were similar to the observations of Zhou et al. [51] in 0.3 M KCl, and very different from the observations of Giménez-Romero et al. [52] at 0.05 M KCl, where CuCl precipitation played an important role. The standard potential for the $Cu^{2+}/[CuCl_2]^-$ system was calculated from the standard potential for Cu^{2+}/Cu^+ (0.159 V [41]) and the complex stability constant from [50] as 0.525 V vs. NHE and thus 0.328 V vs. Ag/AgCl. For the deposition of Cu from $[CuCl_2]^-$ one calculates a standard potential of −0.048 V versus Ag/AgCl.

The change in the shapes of the cyclic voltammograms upon sonication (cf. Fig. 2b, c), the dependency of ε on ultrasound intensity (Fig. 3) and electrode potential (Fig. 4) can be explained by the enhancement of mass transport due to the ultrasound. Immediately before the start of Cu deposition under silent conditions, the electrolyte close to the electrode is enriched with Cu(I) that was formed at higher potentials by reduction of Cu(II). This reduction process is already under mass transport control indicating far-reaching depletion of Cu(II) and enrichment of Cu(I) close to the electrode surface. First Cu deposition therefore proceeds by a one electron transfer reaction from Cu(I), while some Cu(II) is still reduced to Cu(I), which explains ε values close to 1 (Fig. 4). At lower potentials Cu(I) is depleted as well, and reduction now occurs by mass transport limited reduction of Cu(II), and therefore ε approaches 0.5. At these low potentials all incoming Cu(II) ions are reduced to Cu(0). On the reverse sweep, with increasing potentials, only part of the Cu(II) ions reaching the electrode are reduced to Cu(0), and part to Cu(I). Therefore ε decreases to values below 0.5. Finally Cu dissolution starts while the overall currents are still negative, and ε becomes negative. During dissolution of Cu ε values significantly larger than 1 are found in the beginning once the currents are positive. This can be explained by the current-less Cu dissolution through Cu(II) species in solution under the formation of further Cu(I).

In the presence of ultrasound the disappearance of all cathodic peaks together with the strong increase in the cathodic currents can be explained by a gradual transition to charge transfer control due to a strong enhancement in mass transfer [1–4]. In chloride solutions more Cu(II) is reduced to Cu(I) at potentials positive of the Cu deposition, which leads to a strong negative background current. The removal of Cu(I) formed during Cu(II) reduction and during Cu dissolution from the electrode is enhanced as well. Opposite to silent conditions, ε for the deposition started at 0 because of the large currents associated with reduction of Cu(II) to Cu(I). Due to the enhanced mass transport, the accumulation of Cu(I) and depletion of Cu(II) close to the electrode were less. At lower potentials an increasing number of Cu(I) was further reduced to Cu(0), until basically every arriving Cu(II) ion was reduced to Cu. Upon reversal of the sweep direction ε first was similar to the forward sweep. But then electrochemical Cu dissolution to Cu(I) was taking place, while the currents remained negative due to Cu(II) reduction. Therefore ε became negative, and then jumped to positive values as soon as the current became positive (not at very large I_a). The cause for the very large ε values is the continued Cu(II) reduction, which diminishes dQ, while dm is quite large.

Enhanced mass transport keeps the concentration of Cu(II) close to the electrode large, which favours formation of Cu(I), but also Cu corrosion and therefore is detrimental for Cu deposition. In addition the intermediate Cu(I) needed for Cu deposition is removed efficiently from the electrode. This explains why Cu deposition was maximum at low I_a and the total efficiency of the deposition process decreased with I_a. The altered speciation at the surface is also responsible for the more negative start potentials for Cu deposition.

Already for the deposition of pure Co films the composition of the electrolyte has a dramatic influence on the morphology of the layers deposited in the presence of ultrasound (Fig. 9). For the dilute electrolyte an open structure consisting of many spherical entities was formed. In addition, the cyclic voltammogram under silent conditions showed incomplete dissolution of the deposit. Both in absence and presence of ultrasound an electrochemical cathodic reaction at potential positive of Co bulk

deposition was observed connected to a frequency decrease of the resonator and thus a deposition process. This frequency change was larger under silent conditions, and roughly constant under ultrasonication. Explanation of this frequency shift could be the adsorption of some material on the electrode surface. Most probably seems to be the direct deposition of $Co(OH)_2$ based on the following reaction:

$$Co^{2+} + 2H_2O + 2e^- \rightarrow Co(OH)_2 + H_2 \quad (3)$$

The codeposition of hydroxides during electrodeposition of Co has been demonstrated in literature [42]. Under silent conditions strong hydrogen evolution is taking place during the Co metal deposition as well. Due to the absence of stirring this causes a pH increase close to the electrode and further incorporation of $Co(OH)_2$ into the growing deposit. The incorporated $Co(OH)_2$ hinders the dissolution of Co during the anodic peak and is responsible for the irreversible accumulation of material on the electrode in the dilute electrolyte under silent conditions. In the presence of ultrasound the local pH increase is less due to enhanced mass transport, and therefore less $Co(OH)_2$ is embedded in the growing film. However, some deposition according to Eq. (3) is still taking place, and this might explain the widely different film morphology obtained. This material is not removed until all the Co deposited on top has been dissolved, then non-electrochemical dissolution is taking place. This might be assisted by surface cavitation, even though this cannot be proved unequivocally. In the Watts-type electrolyte, the boric acid addition acts as a buffer and prevents both adsorption of $Co(OH)_2$ according to Eq. (3) and the incorporation into the bulk of the material.

The fact that in the presence of CeO_2 in the dilute electrolyte again not the entire deposit is removed from the electrode despite ultrasonic action shows that either the incorporated ceria hinders the dissolution, or that it leads to more $Co(OH)_2$ deposition by influencing the pH changes close to the electrode. Quite interesting are the mass changes outside the electrochemically active areas (Fig. 8b, c): The mass decreases continuously after the end of the anodic dissolution process and before onset of deposition in the second cycle, and there seems to be no potential dependency. The amount of mass removed becomes the larger the larger the ultrasonic intensity is. The most probable explanation of this behavior is the abrasion of material on the electrode by the impact of ceria particles accelerated by acoustic streaming and cavitation in the electrolyte. The formation of ceria/metal nanocomposites is therefore a rather complicated process involving beneficial interactions between ceria and ultrasound that should result in breaking apart of agglomerates (even though this is discussed controversial in [36]) and enhanced transport of ceria towards the electrode, the influence of ultrasound on local pH gradients and on the metal electroplating process, but also the removal of deposit due to abrasion by particle impact and surface cavitation. The choice of electrolyte severely influences the uptake of ceria and alters the morphology. As discussed elsewhere [35], the EQCM technique is not capable of resolving the amount of ceria embedded into the films from the dilute electrolyte due to the deposition of rough and inhomogeneous layers affecting the EQCM response.

The sonoelectrochemical deposition of nanoparticles for subsequent use in fuel cell applications requires the presence of surface active species in the electrolyte. The purpose of these species in the stabilization of the nanoparticles formed in order to prevent their agglomeration and particle growth. However, these additives also influence the electrochemical deposition process itself. This is demonstrated by the very different shape of the cyclic voltammograms from a $CuSO_4$ electrolyte without organic additives and in the presence of PVP (cf. Fig. 10). The difference in the peak shapes as compared to the chloride based system, where the presence of chloride stabilized Cu(I), indicates that PVP stabilized Cu(II). The influence of PVP on electrochemical metal deposition has been discussed in [46, 47], and shall not be discussed here. However, in order to avoid a mere trial and error approach, a detailed understanding would be helpful. Here the EQCM can provide additional information based on the ratio of the mass to charge changes. Figure 10b shows that for potentials above 25 mV during the forward sweep, there is a reduction process taking place that is not connected with the formation of a deposit at all. The pronounced peak is due to deposition of copper on the electrode, and the apparent molar mass M_{app} calculated from the measurement (Eq. (4), same parameters as used in Eq. (2)) is only slightly larger than the true molar mass of copper (66 g mol^{-1} instead of 63.5 g mol^{-1}). This shows that PVP is not embedded in the growing copper film, but at most will be adsorbed at the surface. The peak current increases with increasing ultrasonic intensity (not shown). The fact that the deposition starts at a more positive potential than for the experiment in Fig. 10a can be explained by the different Cu concentration in the electrolytes. However, the intermediate current decrease at lower potentials despite the presence of strong ultrasound and a larger concentration must be caused by the influence of the PVP. At lower potentials, currents increase again, and Cu deposition still is taking place. Now M_{app} is lower than the one for Cu, indicating a reduced current efficiency. During the backward scan deposition continues with $M_{app} = 67.5$ g mol^{-1}. Cu dissolution then proceeds in part by Cu(I) species, leading to a much larger value for M_{app} (86.7 g mol^{-1}). A detailed understanding of the mechanism will require further experiments.

$$M_{app} = -zF \cdot \frac{\Delta m}{\Delta Q} \quad (4)$$

A second complicating factor for the sonotrode based preparation of nanoparticles is the fact that sonotrodes typically are made from a titanium alloy. Already an early

study has demonstrated that these electrodes rather act like semiconductors and that therefore the electrochemical response is very different from metals like platinum [66]. This is the reason for the extreme potentials applied in the literature and in this study. Studies in literature and in this work clearly show that the preparation of nanoparticles in a reasonable size range is possible. However, the deposition of even smaller nanoparticles would be desirable, especially if intended for use as catalyst in PEM fuel cells. This requires a modification of the nucleation and growth behavior and a careful synchronization of ultrasonic pulses and potential pulses. Also shorter pulse durations are required. For the deposition of nanoparticles on well-defined model systems a special potentiostatic method, the so-called double pulse method, has been applied in literature [67–69]. This technique permits to de-couple nucleation and growth, and therefore enables a more accurate fine-tuning of the particle size. Therefore in future work nucleation and growth processes on Ti alloys shall be studied in detail, and the influence of the stabilizers on this behavior shall be explored.

Further aspects for sonoelectrochemical nanoparticle formation are the sonochemical reduction of the metal precursor used, and the analysis of the particle size by DLS in the presence of PVP. Sonochemical reaction alone was observed for the Ag system, however clear differences in the DLS response as compared to the electrochemically treated solutions were seen (not shown). The presence of PVP alone caused particle detection in the DLS system with particle sizes of 8 nm. However, in the presence of metal nanoparticles the PVP signal did not disturb the measurement. Nevertheless, especially for very small particles TEM measurements are necessary and possibly a different type of stabilizer is required.

The application of high intensity ultrasound for the effective decoration of an anode cermet for the SOFC was successful (Fig. 15). This shows that the sonoelectrochemical (or sonochemical) nanoparticle generation followed by decoration of another material is a suitable approach for materials modification at the nanoscale. For the high temperature fuel cell application, the organic material does not affect the performance of the ultimate layer, because it decomposes in thermal post-processing. For low temperature fuel cell applications the presence of the organic compounds could adversely affect the catalytic properties of the nanoparticles [69].

5 Conclusions

Sonoelectrochemistry is a versatile tool for materials synthesis, especially with respect to nanomaterials. It can be combined with the electrochemical quartz crystal microbalance technique for fundamental studies on the influence of ultrasound on the mechanism of electrode reactions that in turn deliver important insight for optimization of materials synthesis. This was shown in this paper by the study of Cu sonoelectrodeposition from chloride electrolytes and from PVP containing electrolytes. There it was possible to determine the current efficiency in situ at different ultrasonic intensities, and to correlate features seen in the sonovoltammogram with deposition processes of certain species like Cu^{2+} or with other processes. This is of significance for optimization of the sonoelectrochemical preparation of colloidal nanoparticle solutions, where without such information synthesis conditions will be based on trial and error. Such colloidal solutions can be used for decoration and thus modification of fuel cell materials, as shown in this work for NiO/GDC powder for solid oxide fuel cell anodes. Another example for the technique was the formation of Co/ceria composites, where interesting information about side reactions was obtained, that would have been unavailable without EQCM.

Acknowledgments Financial funding by the European Union in the framework of the MATSILC (FP6) and the ROBANODE (FP7, JTI FCH-JU) project and by the German Research Foundation is gratefully acknowledged.

References

1. Compton RG, Eklund JC, Marken F (1997) Electroanalysis 9:509
2. Walton DJ (2002) Arkivoc 198
3. Banks CE, Compton RG (2003) Chemphyschem 4:169
4. Pollet B (2012) Power ultrasound in electrochemistry: from versatile laboratory tool to engineering solution. Wiley, Chichester
5. Lauterborn W, Kurz T, Geisler R, Kröninger D, Schanz D (2007) In: Kurz T, Parlitz U, Kaatze U (eds) Oscillations, waves, and interactions. Universitätsverlag Göttingen, Göttingen, p 139
6. Thompson LH, Doraiswamy LK (1999) Ind Eng Chem Res 38:1215
7. Suslick KS, Flannigan DJ (2008) Annu Rev Phys Chem 59:659
8. Neppiras EA (1980) Phys Rep 61:159
9. Banks CE, Compton RG (2003) Electroanalysis 15:329
10. del Campo FJ, Melville J, Hardcastle JL, Compton RJ (2001) J Phys Chem A 105:666
11. Ashokkumar M, Grieser F (2007) Phys Chem Chem Phys 9:5631
12. Suslick KS, Price GJ (1999) Annu Rev Mater Sci 29:295
13. Crum LA (1995) Ultrason Sonochem 2:S147
14. Maisonhaute E, Brookes BA, Compton RG (2002) J Phys Chem B 106:3166
15. Cooper EL, Coury LA (1998) J Electrochem Soc 145:1994
16. Kumar A, Gogate PR, Pandit AB (2007) Ind Eng Chem Res 46:4368
17. Sato M, Fujii T (2001) Phys Rev E 64:026311
18. Touyeras F, Hihn JY, Bourgoin X, Jacques B, Hallez L, Branger V (2005) Ultrason Sonochem 12:13
19. Delplancke JL, Dille J, Reisse J, Long GJ, Mohan A, Grandjean F (2000) Chem Mater 12:946
20. Reisse J, Caulier T, Deckerkheer C, Fabre O, Vandercammen J, Delplancke JL, Winand R (1996) Ultrason Sonochem 3:S147

21. Yin B, Ma H, Wang S, Chen S (2003) J Phys Chem B 107:8898
22. Reisse J, Francois H, Vandjzrcammen J, Fabre O, Kirsh-De Mesmaeker A, Maerschalk C, Delplancke JL (1994) Electrochim Acta 39:37
23. Aqil A, Serwas H, Delplancke JL, Jerome R, Jerome C, Canet L (2008) Ultrason Sonochem 15:1055
24. Shen Q, Min Q, Shi J, Jiang L, Hou W, Zhu JJ (2011) Ultrason Sonochem 18:231
25. González-García J, Esclapez MD, Bonete P, Hernández YV, Garretón LG, Sáez V (2010) Ultrasonics 50:318
26. Pollet BG (2010) Int J Hydrogen Energy 35:11986
27. Saez V, Mason TJ (2009) Molecules 14:4248
28. Wagner FT, Lakshmanan B, Mathias MF (2010) J Phys Chem Lett 1:2204
29. Garbellini GS, Salazar-Banda GR, Avaca LA (2010) Port Electrochim Acta 28:405
30. Siddique M, Farooq R, Khan ZM, Khan Z, Shaukat SF (2011) Ultrason Sonochem 18:190
31. Yasman Y, Bulatov V, Gridin VV, Agur S, Galil N, Armon R, Schechter I (2004) Ultrason Sonochem 11:365
32. Goldcamp MJ, Underwood MN, Cloud JL, Harshman S, Ashley K (2008) J Chem Educ 85:976
33. Walker R (1997) Ultrason Sonochem 4:39
34. Asami R, Fuchigami T, Atobe M (2006) Langmuir 22:10258
35. Argirusis C, Matić S, Schneider O (2008) Phys Stat Sol A 205:2400
36. Lee D, Gan YX, Chen X, Kysar JW (2007) Mater Sci Eng A 447:209
37. Schneider O, Martens S, Argirusis C (2009) ECS Trans 16(25):107
38. Ff Xia, Wu Mh, Wang F, Jia Zy, Wang Al (2009) Curr Appl Phys 9:44
39. Gül H, Kılıç F, Aslan S, Alp A, Akbulut H (2009) Wear 267:976
40. Schneider O, Matić S, Argirusis C (2008) Electrochim Acta 53:5485
41. Bard AJ, Faulkner LR (2001) Electrochemical methods: Fundamentals and applications, 2nd edn. Wiley, New York
42. Matsushima JT, Trivinho-Strixino F, Pereira EC (2006) Electrochim Acta 51:1960
43. Margulis MA, Margulis IM (2003) Ultrason Sonochem 10:343
44. Margulis IM, Margulis MA (2005) Acoust Phys 51:695
45. Sauerbrey G (1959) Z Phys 155:206
46. Haas I, Shanmugam S, Gedanken A (2006) J Phys Chem B 110:16947
47. Yin B, Ma HY, Wang SY, Chen SH (2003) J Phys Chem B 107:8898
48. Liu YC, Lin LH, Chiu WH (2004) J Phys Chem B 108:19237
49. Unger B, Hähnert M, Nitzsche R (1998) J Sol-Gel Sci Technol 13:81
50. Kekesi T, Isshiki M (1997) J Appl Electrochem 27:982
51. Zhou M, Myung N, Chen X, Rajeshwar K (1995) J Electroanal Chem 398:5
52. Giménez-Romero D, Gabrielli C, García-Jareño JJ, Perrot H, Vicente F (2006) J Electrochem Soc 153:J32
53. Nwoko VO, Shreir LL (1973) J Appl Electrochem 3:137
54. Hovestad A, Janssen LJJ (1995) J Appl Electrochem 25:519
55. Kim MH, Hong MZ, Kim YS, Park E, Lee H, Ha HW, Kim K (2006) Electrochim Acta 51:6145
56. Cârâc G, Benea L, Iticescu C, Lampke T, Steinhäuser S, Wielage B (2004) Surf Eng 20:353
57. Lampke T, Wielage B, Dietrich D, Leopold A (2006) Appl Surf Sci 253:2399
58. Qu NS, Zhu D, Chan KC (2006) Scr Mater 54:1421
59. Escudero MJ, Irvine JTS, Daza L (2009) J Power Sources 192:43
60. Gong M, Liu X, Trembly J, Johnson C (2007) J Power Sources 168:289
61. Park SD, Vohs JM, Gorte RJ (2000) Nature 404:265
62. Gorte RJ, Kim H, Vohs JM (2002) J Power Sources 106:10
63. Gavrielatos I, Drakopoulos V, Neophytides S (2008) J Catal 259:75
64. Corbierre MK, Cameron NS, Lennux RB (2004) Langmuir 20:2867
65. Mancier V, Daltin AL, Leclercq D (2008) Ultrason Sonochem 15:157
66. Compton RG, Eklund JC, Marken F, Waller DN (1996) Electrochim Acta 41:315
67. Ueda M, Dietz H, Anders A, Kneppe H, Meixner A, Plieth W (2002) Electrochim Acta 48:377
68. Sandmann G, Dietz H, Plieth W (2000) J Electroanal Chem 491:78
69. Brülle T, Ju W, Niedermayr P, Denisenko A, Paschos O, Schneider O, Stimming U (2011) Molecules 16:10059